

## NONLINEAR OPTICAL PROCESSES MANIFESTING AS ANDERSON LOCALIZATION OF LIGHT IN MESOSCOPIC MATERIALS

Ioan BALTOG<sup>1</sup>, Mihaela BAIBARAC<sup>1</sup>, Lucian MIHUT<sup>1</sup>, Ion SMARANDA<sup>1</sup>, Serge LEFRANT<sup>2</sup>

<sup>1</sup>National Institute of Materials Physics, P.O. Box MG-7, Bucharest, R-77125, Romania

<sup>2</sup>Institut des Matériaux “Jean Rouxel”, 2 rue de la Houssinière, B.P. 32229, F-44322, Nantes, France

E-mail: ibaltog@infim.ro

Abnormal anti-Stokes Raman emission (AASRE) is defined by an anti-Stokes/Stokes intensity ratio much greater than expected on the basis of the equilibrium population of excited vibration states provided by the Boltzmann law. AASRE can be observed both in materials with intrinsic nonlinear optical properties as LiNbO<sub>3</sub> or materials in which the nonlinear optical properties are induced by resonant optical excitation, as carbon nanotubes. Using a surface enhanced Raman scattering (SERS) device, consisting from single wall carbon nanotubes deposited on a rough Au or Ag support and LiNbO<sub>3</sub> in form of powder, we demonstrate that under continuous single beam excitation they present AASRE whose properties are similar to a single beam pumped Coherent Anti-Stokes Raman Scattering. AASRE is usually accompanied by a coherent backscattering, it can be considered as Anderson localization of light that results from a wave-mixing mechanism of the incident laser light with a Stokes shifted Raman light produced by a spontaneous Raman light scattering process. The transport of the light inside of sample, giving rise to AASRE and coherent backscattering, is done by an elastic light scattering mechanism.

*Key words:* Raman scattering, coherent anti-Stokes Raman scattering, coherent backscattering, Anderson localization of light.

### 1. INTRODUCTION

In recent years, a subject much debated in the field of Raman spectroscopy refers to the appearance of anomalous anti-Stokes Raman emission (AASRE) [1-6]. The term AASRE defines an anti-Stokes Raman emission for which the anti-Stokes/Stokes intensity ratio ( $I_{aS}/I_S$ ) is much greater than expected on the basis of the equilibrium population of the excited vibration states provided by the Boltzmann law:

$$\frac{I_{aS}}{I_S} = \left( \frac{\sigma(\alpha_\Omega)_{aS}}{\sigma(\alpha_\Omega)_S} \right) \left( \frac{\omega_l + \Omega}{\omega_l - \Omega} \right)^4 \exp\left( \frac{h\Omega}{kT} \right)^{-1}. \quad (1)$$

In equation (1),  $\omega_l$  and  $\Omega$ ,  $h$ ,  $k$  and  $T$  are the wavenumbers of excitation light and Raman line (cm<sup>-1</sup>), the Planck constant, the Boltzmann constant and temperature, respectively. Illustratively, in Eq.2 the terms  $\sigma(\alpha_\Omega)_{aS}$  and  $\sigma(\alpha_\Omega)_S$  indicate the anti-Stokes and the Stokes cross sections associated with the  $\Omega$  wavenumber. These terms depend on the polarizability of material, being equal for the normal (non-resonant) spontaneous Raman process. A review of the literature devoted to this subject indicates that, on one hand, AASRE was commonly seen in carbon nanotubes [4–11] while on the other that it was mostly observed when a SERS measurement configuration was used [1–3, 12–16]. The results obtained in the latter case was interpreted by a no thermal population of the higher vibration states induced by a large photon density of the excitation light combined with an enhancement of the Raman cross section [2]. An answer to the question why AASR appears only in these two cases we try to give in the follows.

The above mentioned studies have revealed that AASRE is conditioned by the presence of a resonant optical excitation process which can be created directly when the exciting light produces an electronic transition between two electronic levels of the studied material, for example the inter-band transitions

between the van Hove density of states singularities of carbon nanotubes [17], or indirectly by a surface enhanced Raman scattering (SERS) mechanism, when the large anti-Stokes intensities observed result from a resonant Raman process occurring in the adsorbate-metallic surface complex for which the Stokes and anti-Stokes Raman cross-sections are not equivalent. Another detail, yet unnoticed, refers to the sample morphology. Both carbon nanotubes, which are in form of powder and SERS measuring supports for which the dominant structure is imposed by the roughness of the metal substrate, are morphological configurations that strongly scatter light. Figure 1, obtained by Scanning Electron Microscopy (SEM), illustrates this type of morphologies in which the light scattering units are smaller than the wavelength of the visible optical spectrum.

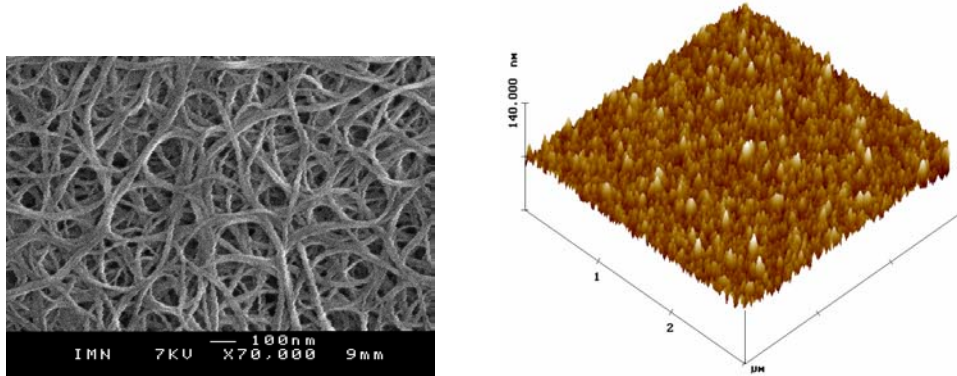


Fig. 1 – The main morphological forms for which it was observed AASRE: carbon nanotubes powder (left) and SERS support (right).

Recently, using the resonant optical excitation and SERS measuring technique, AASRE was also found in other materials. Scrupulous investigation revealed new dependences for AASRE emission: *i*) the intensity of anti-Stokes Raman lines increases with the vibrational wavenumber; *ii*) a square dependence on the film thickness; *iii*) a square dependence on the exciting laser intensity; *iv*) a linear dependence on the numerical aperture ( $NA$ ) of the microscope objective used for the detection of the anti-Stokes emission; *v*) the polarization ratio on the anti-Stokes side is always greater in comparison with that measured for a spontaneous Stokes Raman emission [18–20]. All these features cannot be entirely explained by existing theories associated with a resonant Raman effect or SERS mechanism and surprisingly, they are rather associated to a reminiscent single beam CARS process. Evidently, such an explanation should be treated with caution knowing that until now the single beam CARS process has not been reported other than using a femtosecond-high intensity pulse laser as excitation light source, combined with control pulse-shaping techniques or noise autocorrelation spectroscopy. In these schemes, a single femtosecond pulse simultaneously provides the necessary pump, Stokes and probe photons [21–24].

Raman light scattering is one example of a complex interaction between the incident electromagnetic wave (EM) and the material's molecular/atomic structure. Under the oscillating EM field of the exciting light a periodic separation of charge results in the electron cloud which is called an induced molecular dipole moment,  $P$ . The oscillating induced dipole moment manifests itself as a source of secondary EM radiation, thereby resulting in scattered light. The strength of the induced dipole moment,  $P$ , is given by  $P = \alpha E$ , where  $\alpha$  is the polarizability and  $E = E_0(\cos 2\omega_0 t + \varphi_0)$  is the strength of electric field of the incident EM wave. On the macroscopic scale, the response of a material to resonant EM excitation is described by polarization  $P = P_0 + \chi^{(1)} E + \chi^{(2)} EE + \chi^{(3)} EEE + \dots$  followed by higher order terms. Thus, the terms of higher order as  $\chi^{(2)} EE$  and  $\chi^{(3)} EEE$  that appears in the polarization expression amount to fulfilling the key condition to generate a nonlinear optical process [25, 26], they summarize the contribution of two effects, one related to the resonant electronic excitation, when  $\chi^{(2)}$ ,  $\chi^{(3)}$  become different from zero and another to the electromagnetic field confinement. In this context, two main questions rise: *i*) if AASRE can be simulated with a single beam CARS process, then it should be observed both on nonlinear optical materials that intrinsically have  $\chi^{(3)} \neq 0$  and materials that become nonlinear under resonant optical excitation; *ii*) if the appearance of AASRE depends on the scattering properties of the sample, then its intensity must be modified by sample morphology.

Coherent Anti-Stokes Raman Scattering (CARS) is a nonlinear process of third order, in which the anti-Stokes light  $\omega_{as}$  results from the parametric coupling of the incident laser light  $\omega_l$ , the Stokes light ( $\omega_s = \omega_l - \Omega$ ) where  $\Omega$  is the frequency of the coherently excited molecular vibration and a probe light  $\omega_p$ . If  $\omega_l = \omega_p$ , the CARS experiment appears as a degenerate four-wave mixing process that reduces to an energy transfer between the two pump waves,  $\omega_l$  and  $\omega_s$ . In the plane-wave approximation and for a non-absorbing medium, the time averaged CARS signal intensity is given by Eq. (2):

$$I_{CARS} \approx N_A \omega_{AS}^2 d^2 |\chi^{(3)}|^2 I_l^2 I_s \frac{\sin^2(\Delta k L / L)}{(\Delta k L / L)}. \quad (2)$$

It reveals particular dependences of the anti-Stokes Raman intensity on the anti-Stokes Raman shift  $\omega_{as}$ , the sample slab thickness  $d$ , the incident pump intensity  $I_l$ , the third order nonlinear dielectric susceptibility  $\chi^{(3)}$ , the numerical aperture  $N_A$  of the collecting lens. The coherent nature of the CARS process is reflected by fulfilling the phase-matching condition  $|\Delta k| \cdot L \ll \pi$ , where  $L$  is the interaction length between the mixing light beams and  $\Delta k = k_{as} - (2k_p - k_s)$  and  $k_{as}$ ,  $k_s$  and  $k_p$  are the wave vectors of the anti-Stokes, Stokes and pump light, respectively [25, 26]. A good phase matching is achieved for  $\Delta k = 0$ . For condensed media  $\Delta k \approx 0$  is fulfilled if the beams cross at an angle  $\theta$ . For tightly focused beams this requirement relaxes, being no longer sensitive to the Raman shift and so, a CARS spectrum can be observed at an angle  $\theta_{as}$  larger than the Stokes angle  $\theta_s$  [27, 28].

In the following we demonstrate that the AASRE emerging from a mesoscopic material can actually be treated as a single beam CARS process, conditioned by  $\chi^{(3)} \neq 0$  and a particular morphology of the sample in which a favorable CARS phase matching geometry between the incident laser light and Stokes Raman emission is achieved by a light scattering mechanism.

## 2. EXPERIMENTAL

Raman spectra were recorded at room temperature in air, in a backscattering geometry, using a Jobin Yvon T64000 Raman-spectrophotometer equipped with a standard microscope objective  $\times 50$  and  $\times 10$  of numerical aperture 0.55 and 0.25 that provide collection light cones of 28.9 and 66.7 degrees, respectively. The microscope system permitted the image of the laser spot on the sample to be recorded. The intensity of the laser excitation light (Argon: 514.5 nm or Krypton: 676.4 nm) was adjusted to avoid the irreversible transformation of the samples. Materials used were single wall carbon nanotubes (SWNTs) prepared by arc discharge of ALDRICH-SIGMA provenience and  $\text{LiNbO}_3$  in form of single crystal and micrometric powder ( $< 20\mu\text{m}$ ) prepared by ball milling, respectively. SWNTs were investigated by SERS technique, using films of 30–150 nm thick deposited on an active (Au or Ag) SERS support. SWNTs films were obtained by evaporating a solvent (toluene) from a uniformly distributed emulsion of nanotubes on rough metallic substrates. Gold and silver SERS active substrates, with a mean roughness of about 150 nm, were prepared by vacuum evaporation [29]. Coherent backscattering measurements on  $\text{LiNbO}_3$  powder and  $\text{LiNbO}_3$  platelets obtained by non-hydrostatic compression of the powder, were performed at Argon laser line of  $\lambda_{\text{exc}} = 476$  nm with an homemade experimental set up, similar with that described in Ref. [30].

## 3. DISCUSSION

Figure 2 presents the anti-Stokes and Stokes SERS spectra of SWNTs situated in the 1 100–1 700  $\text{cm}^{-1}$  spectral interval. Two bands are found, a broad one, labeled “G band” is associated with the tangential stretching modes (TM) and other, frequently referred as the “D band”, not intrinsically related to the nanotube structure because it appears also in the Raman spectrum of other graphitic materials, is an indicative of disorder induced in the graphitic lattice or defects in nanotubes [17]. Under excitation energy

between 1.5 and 2.2 eV the G band shows a wide asymmetric profile towards lower wavenumbers with a maximum at  $\sim 1540 \text{ cm}^{-1}$ , it indicating the resonant optical excitation of metallic nanotubes. Estimation of AASRE done for the G band by the ratio  $I_{aS}/I_{Boltzmann}$  at resonant ( $\lambda_{exc} = 676.4 \text{ nm}$ ) and less resonant ( $\lambda_{exc} = 514.5 \text{ nm}$ ) excitation wavelengths lead to the values of 2.747 and 70, respectively, which are much bigger than 1 if  $I_{aS}$  is determined by the Boltzmann law, i.e., eq. (1). Figure 2 discloses a subtle variation of the Raman intensities as function of the film thickness: the highest intensity is observed for the thinnest films in the Stokes branch while in the anti-Stokes branch for the thickest film.

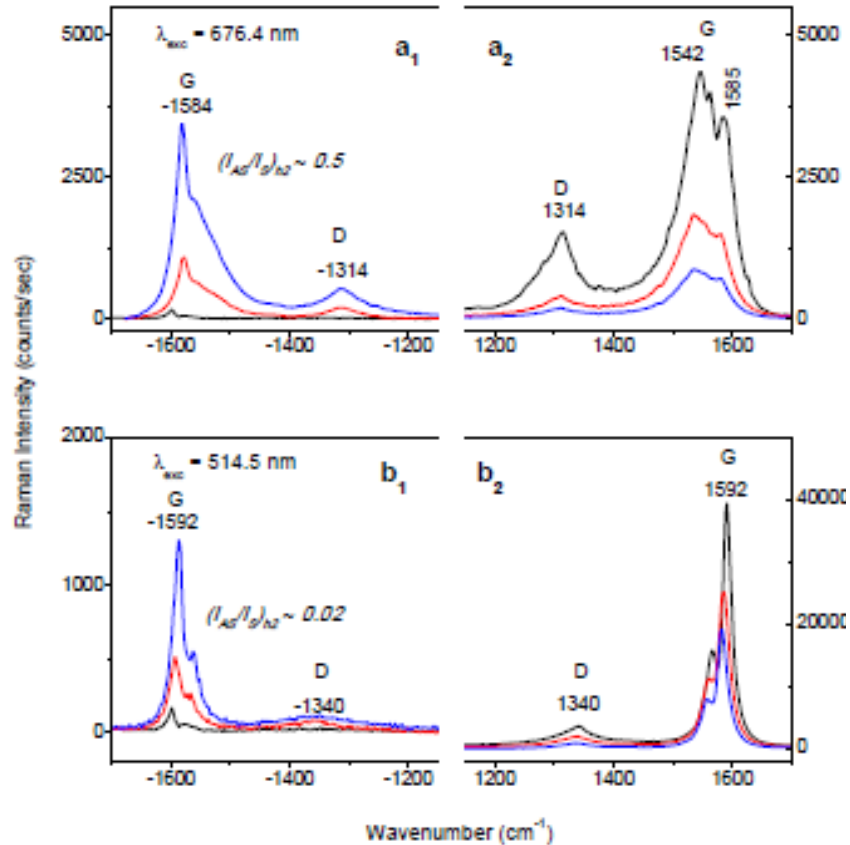


Fig. 2 – Stokes ( $a_2; b_2$ ) and anti-Stokes ( $a_1; b_1$ ) SERS spectra on SWNTs films of different thickness i.e., 30, 60 and 120 nm (black, red, blue) recorded through a microscope objective of  $\times 55$  numerical aperture under resonant (676.4 nm) and non-resonant (514.5 nm) excitation wavelengths. AASRE is estimated by  $I_{aS}/I_{Boltzmann}$  ratio of G band. Au was used as metallic SERS supports.

According with eq. (2), this particular dependence on the film thickness is a powerful argument that in the Stokes and anti-Stokes branches operates efficiently two enhancement processes, SERS and CARS respectively. The existence of a CARS process, more precise a degenerate four waves mixing process, requires intrinsically two exciting lights,  $\omega_l$  of the pump laser and  $\omega_s$  furnished by a SERS process. This is experimentally confirmed for SWNTs film deposited on a silicon support, unable to produce a SERS enhancement as shown in Ref.18. With regard to Fig. 2, must be mentioned as significant detail the fact that it was obtained on samples characterized by a great power of scattering of light, which are built as a layer of SWNTs (see Fig. 1, left) deposited on a metallic rough SERS support (see Fig.1, right).

Figure 3 reveals an interesting result. According to expectation, it demonstrates that this effect can be also observed without resonant excitation, on other materials, which intrinsically have  $\chi^{(3)} \neq 0$  and an example is  $\text{LiNbO}_3$ . If  $I_{Boltzmann}$  indicates the anti-Stokes replica (red curves) calculated with eq. (1) applied to the recorded Stokes spectra, then AASRE may be also estimated by the ratio  $I_{aS}/I_{Boltzmann}$  associated to different Raman lines. A supplementary requirement concerning the occurrence of this effect is the sample morphology, namely its capability to ensure a strong background of scattered light. Convincing arguments in this sense are furnished by Fig. 3 in which the Stokes and anti-Stokes Raman spectra of  $\text{LiNbO}_3$  are

displayed in three morphological forms: single crystal, platelet made from micrometric powder compressed non-hydrostatically at 0.58 GPa and uncompressed powder ( $< 40 \mu\text{m}$ ). The optical microscopic images of Fig. 3 highlight two extreme situations in the observation of AASRE; one is the case of  $\text{LiNbO}_3$  single crystal, characterized by a very low background of light scattering, when AASRE does not exist and the recorded anti-Stokes Raman spectrum coincides with the calculated spectrum applying the Boltzmann formula to the Stokes spectrum (Fig. 3, red curve) and another when AASRE is observed if the measurements were made on  $\text{LiNbO}_3$  powder.

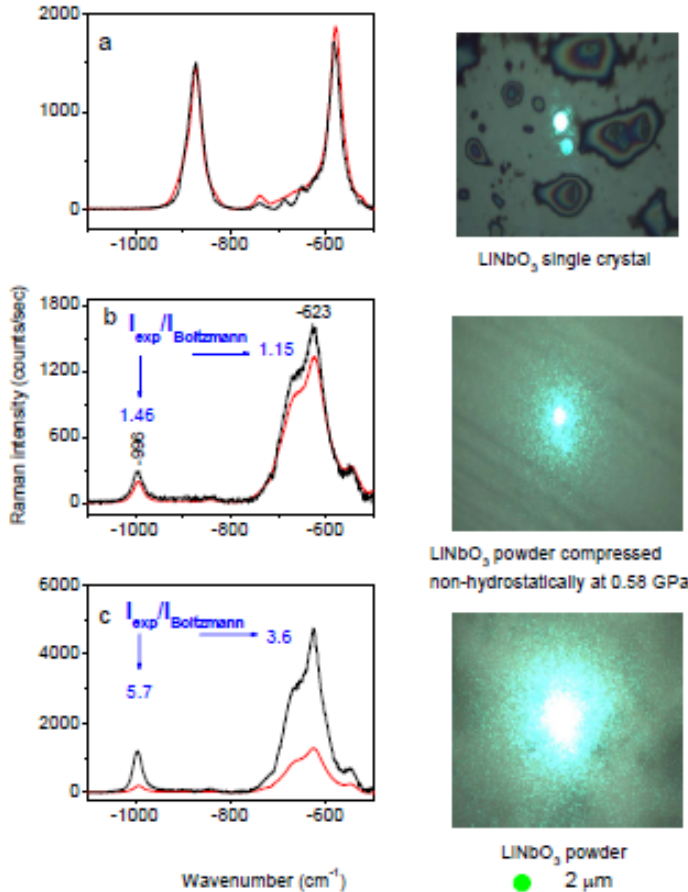


Fig. 3 – Anti-Stokes Raman spectra at  $\lambda_{\text{exc}} = 514.5 \text{ nm}$  of  $\text{LiNbO}_3$  in three morphological forms: a) single crystal; b) platelet made from  $\text{LiNbO}_3$  powder compressed non hydrostatically at 0.58GPa; c) micrometric ( $< 40 \mu\text{m}$ )  $\text{LiNbO}_3$  powder. Red lines show the anti-Stokes replica calculated with the Boltzmann formulae applied to the recorded Stokes spectra. On the right side are shown the optical microscopic images of the laser spot focused on the respective samples. The illuminated area indicates a stronger backscattering process which occurs into a narrow cone of few degrees opening. Small green circle indicates the diameter of the laser spot. All experimental Raman data were obtained with a microscope objective of 0.55 numerical apertures.

An intermediate situation is that of  $\text{LiNbO}_3$  platelet prepared by non-hydrostatic compression at 0.58 GPa in which the particles close-packed scatter the light less. In this context, the dependence of AASRE on the sample morphology is tempted to be viewed as similar to other optical processes developed in mesoscopic materials like optical coherent backscattering (CBS) or random lasers [30, 31].

The deduction is supported by Fig. 5, which demonstrates the occurrence of CBS effect in  $\text{LiNbO}_3$  as powder and platelet obtained by non-hydrostatic compression of the powder at 0.58 GPa. Coherent backscattering is a phenomenon in which a coherent radiation (such as a laser beam) propagates through a medium that contains a large number of scattering centers of size comparable to the wavelength. Due to the reciprocity of light propagation, such paths will always have a counterpart of exactly the same length, which implies that they will interfere constructively in the backward direction leading to the appearance of a narrow intensity cone whose height is predicted to be twice the incoherent background level [32]. This effect is known as Anderson localization of light. As disorder or roughness increase, the probability of forming closed loops on which intensity is enhanced. This critical amount of disorder has been estimated the mean free path ( $l^*$ ) roughly equals the inverse wavenumber, i.e. when  $kl^* \sim 1$ . Such a mechanism was first proposed for the transport of electrons in metals, where it was found that an increase in disorder can turn a metal into an insulator [33].

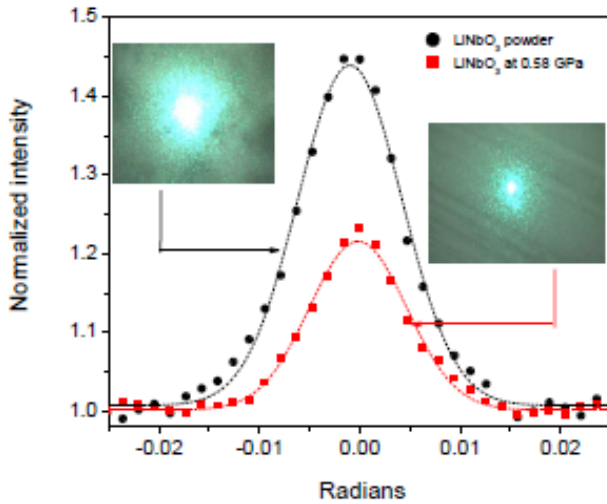


Fig. 4 – Coherent backscattering of  $\lambda_{exc} = 476$  nm laser light on  $\text{LiNbO}_3$  powder (black) and platelet (red) obtained by non-hydrostatic compression at 0.58 GPa.

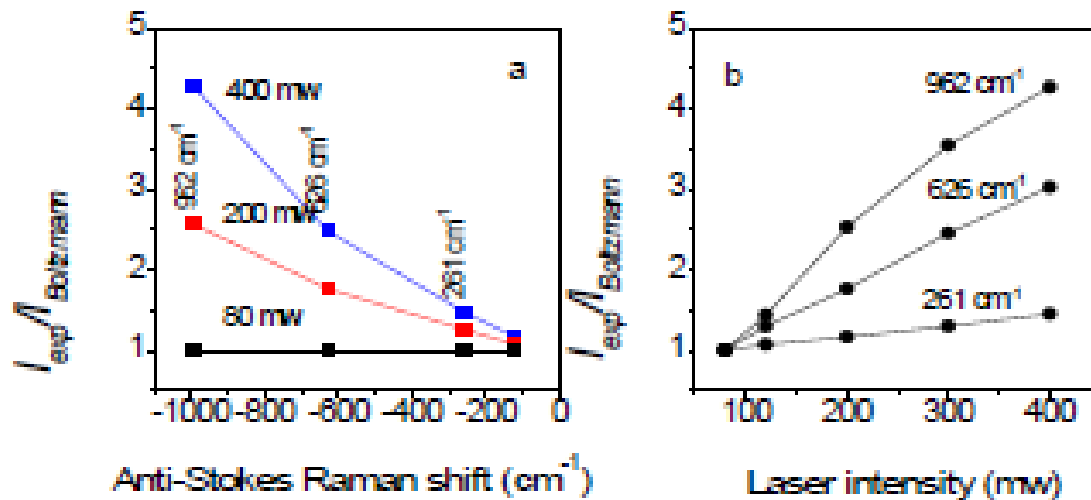


Fig. 5 – AASRE observed in backscattering geometry on a nonlinear optical material (powder of  $\text{LiNbO}_3$ ) at  $\lambda_{exc}=514.5$  nm. In panels (a) and (b) are presented two characteristics of the AASRE: the increase of the ratio  $(I_{exp}/I_{Boltzmann})_{as}$  with the Raman shift and exciting laser intensity, respectively. All experimental Raman data were obtained with a microscope objective of 0.55 numerical aperture.

Figure 5 reveals for  $\text{LiNbO}_3$  powder two properties of AASRE, which were previously found by resonant SERS studies on other materials: one refers to the fact that the anti-Stokes emission grows non-uniformly along the Raman spectrum, the lines of higher wavenumber increase more than the lines of smaller wavenumber [3, 12, 18] and another that the intensity of anti-Stokes Raman lines increases differently with the exciting laser intensity, the lines of smaller wavenumber increase less than the lines of higher wavenumber, the latter revealing a dependence close to a quadratic one [2, 18].

Another property already revealed in Ref. [18] regards the increase of AASRE intensity with the numerical aperture (NA) of the microscope objective used for its detection. In fact, this indicates that the anti-Stokes emission is not uniform in all space as in the case of a spontaneous Raman emission, it has a dominant grazing component.

Figure 6 depicts this property in the case of  $\text{LiNbO}_3$  powder; it shows a strong enough AASRE and its absence when the detection was performed through an objective of numerical aperture  $\times 50$  and  $\times 10$ , respectively. Higher numerical aperture allows increasingly oblique rays to enter the objective front lens, producing a more highly signal. The use of higher aperture should lead to stronger Raman signal both in the Stokes and anti-Stokes branches, fact that in reality does not happen. Experimentally, one observes that using an objective of higher numerical aperture (i.e.,  $\times 50$ ) the anti-Stokes Raman signal increases more, this indicating that AASRE emerges from the sample by a more complicated mechanism than the spontaneous Raman emission.

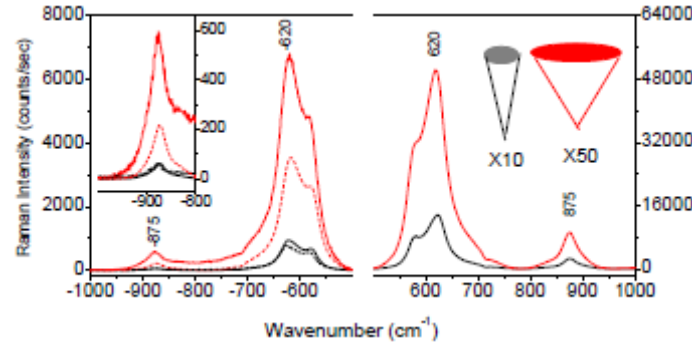
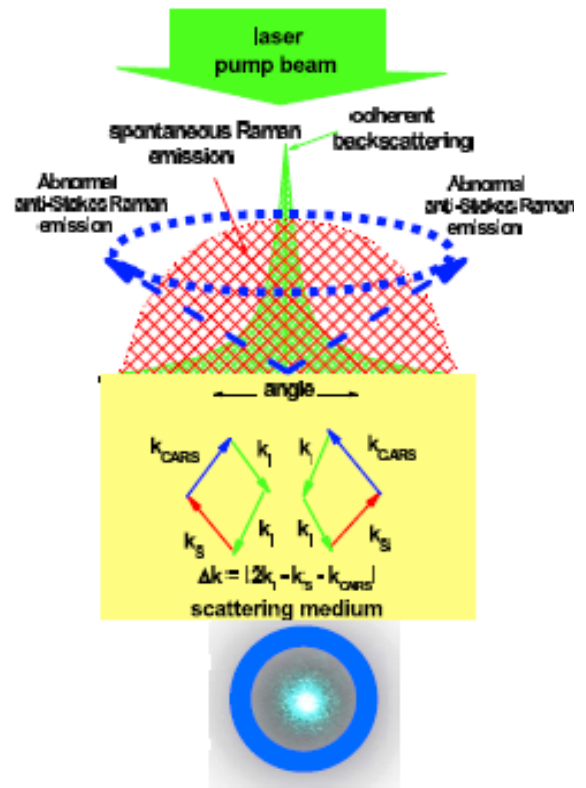


Fig. 6 – Stokes and anti-Stokes Raman spectra at  $\lambda_{exc} = 514.5$  nm of  $\text{LiNbO}_3$  powder recorded in backscattering geometry through a microscope objective of different NA, 0.25 (solid black curves) and 0.55 (solid red curves). Dashed curves show the anti-Stokes spectra, for the two NA used.

Fig. 7 – Scheme of anomalous anti-Stokes Raman emission (blue circle) and backscattering effect of generated by laser excitation beam (central green spot).



According with Eq. 2 we are tempted to consider a nonlinear optical phenomenon, reminiscent of a single beam CARS effect. The incident laser light absorbed in the diffusive medium gives rise to a high light scattering background, which is viewed outside the sample as a coherent backscattering in a narrow cone of several degrees and a spontaneous Raman light, which a part leaves the sample in all directions and another part is in turn strongly scattered inside the medium. Thus, each particle of the medium is submitted simultaneously to two irradiation fields, one of the incident laser light,  $\omega_l$  and another of the Stokes shifted Raman light,  $\omega_s$ , which in particular conditions may mix together generating a CARS type emission. For these two key requirements must be necessarily fulfilled: a non-zero electric susceptibility of third order,  $\chi^{(3)} \neq 0$ , and a sample morphology suitable<sup>(3)</sup> to ensure the formation of a favorable phase-matching geometry by a multiple scattering process. A powder morphological form is characterized by a high power of light scattering. If the maximum path difference  $a$  between the constituent particles is smaller than the excitation wavelength  $\lambda_{exc}$ ,  $a < \lambda_{exc}$ , the scattered waves may interfere constructively giving rise to the coherent backscattering. In this context one can easily imagine the possibility of formation of a CARS favorable phase

matching geometry between the excitation laser light and Stokes Raman light, the former emerging as coherent backscattering and the latter extending inside the sample in all directions and angles. The change in the arrangement of nanoscaled structures may change the probability of formation of such phase matching geometry, a situation which would be reflected in a decrease of CARS intensity. Figure 7 shows schematically the occurrence of such a process [34]. The former requirement may satisfy both of the materials possessing intrinsic nonlinear properties and the materials that gain such properties by resonant optical excitation. Regarding the morphology of the sample, it must be characterized by a high power of light scattering and powders and rough surfaces appears as the most indicated morphological forms in the AASRE generation. The interference effects are crucial to light localization in a disordered medium, they require length scale  $a < \lambda_{ex}$  easy accomplished in the case of powders. In condensed media, due to the small dispersion of refractive index over small paths, the phase matching condition may be fulfilled in geometry when the beams cross at an angle  $\theta$ . Such geometry determines for AASRE a different spatial distribution in comparison with the spontaneous Raman scattering, the former emerges grazing the surface sample while the latter propagates in all space. In accordance with Eq. (1), such a property is evidenced by a dependence of the AASRE intensity on the numerical aperture of the microscope objective used for detection.

#### 4. CONCLUSIONS

The scope of this work was to demonstrate that under continuous single beam excitation an intense AASRE may be generated that has the characteristics of a single beam excited broadband CARS process. This is the first time that such an emission has been revealed on  $\text{LiNbO}_3$  which possess intrinsic nonlinear optical properties,  $\chi^{(3)} \neq 0$ . The corroboration of the anti-Stokes spectra with optical microscopic images and coherent backscattering studies reveals that the appearance of AASRE is strongly dependent on the sample morphology, the powders being the most suitable morphological forms. The similarity of AASRE to a single-beam CARS was demonstrated by *i*) its increasing intensity with the vibrational wavenumber; *ii*) its nonlinear dependence on the exciting laser intensity; *iii*) its dependence on the numerical aperture (NA) of the microscope objective used for the detection of the anti-Stokes emission.

#### ACKNOWLEDGMENTS

This work was financed by the Romanian research project IDEI 77/2011.

#### REFERENCES

1. E. J. LIANG, A. WEIPPERT, J.-M. FUNK, A. MATERNY, W. A. KIEFER, *Experimental observation of surface-enhanced coherent anti-Stokes Raman scattering*, Chem. Phys. Lett., **227**, pp.115–120, 1994.
2. K. KNEIPP, Y. WANG, H. KNEIPP, I. ITZKAN, R. R. DASARI, M. S. FELD, *Population Pumping of Excited Vibrational States by Spontaneous Surface-Enhanced Raman Scattering*, Phys. Rev. Lett., **76**, pp. 2444–2447, 1996.
3. T. L. HASLETT, L. TAY, M. MOSKOVITS, *Can surface-enhanced Raman scattering serve as a channel for strong optical pumping?*, J. Chem. Phys., **113**, pp.1641–1646, 2000.
4. K. KNEIPP, H. KNEIPP, P. CORIO, S. D. M. BROWN, K. SHAFER, J. MOTZ, L. T. PERELMAN, E. B. HANLON, A. MARUCCI, G. DRESSELHAUS, M. S. DRESSELHAUS, *Surface-Enhanced and Normal Stokes and Anti-Stokes Raman Spectroscopy of Single-Walled Carbon Nanotubes*, Phys. Rev. Lett., **84**, pp. 3470–3473, 2000.
5. P. H. TAN, Y. TANG, C-Y. HU, F. LI, Y. L. WEI, H. M. CHENG, *Identification of the conducting category of individual carbon nanotubes from Stokes and anti-Stokes Raman scattering*, Phys. Rev. B, **62**, pp. 5186–5190, 2000.
6. P. V. TEREDESAI, A. K. SOOD, A. GOVINDARAJ, C. N. R. RAO, *Surface enhanced resonance Raman scattering from radial and tangential modes of semiconducting single wall carbon nanotubes*, Appl. Surf. Sci., **182**, pp.196–201, 2001.
7. V. ZOLYOMI, J. KURTI, *Calculating the discrepancy between the Stokes and anti-Stokes Raman D band of carbon nanotubes using double resonance theory*, Phys. Rev. B, **66**, 073418, 2002.
8. S. L. ZHANG, X. HU, H. LI, Z. SHI, K. T. YUE, J. ZI, Z. GU, X. WU, Z. LIAN, Y. ZHAN, F. HUANG, L. ZHOU, Y. ZHANG, S. IJIMA, *Abnormal anti-Stokes Raman scattering of carbon nanotubes*, Phys. Rev. B, **66**, 035413, 2002.
9. P. H. TAN, L. AN, L. Q. LIU, Z. X. GUO, R. CZERW, D. L. CARROLL, P. M. AJAYAN, H. L. GUO, *Probing the phonon dispersion relations of graphite from the double-resonance process of Stokes and anti-Stokes Raman scatterings in multiwalled carbon nanotubes*, Phys. Rev. B, **66**, 245410, 2002.

10. L. G. CANÇADO, M. A. PIMENTA, R. SAITO, A. JORIO, L. O. LADEIRA, A. GRUENEIS, A. G. SOUZA-FILHO, G. DRESSELHAUS, M. S. DRESSELHAUS, *Stokes and anti-Stokes double resonance Raman scattering in two-dimensional graphite*, Phys. Rev. B, **66**, 035415, 2002.
11. A. G. SOUZA FILHO, S. G. CHOU, GE. G. SAMSONIDZE, G. DRESSELHAUS, M. S. DRESSELHAUS, L. AN, J. LIU, A.K. SWAN, M. S. ÜNLÜ, B. B. GOLDBERG, A. JORIO, A. GRÜNEIS, R. SAITO, *Stokes and anti-Stokes Raman spectra of small-diameter isolated carbon nanotubes*, Phys. Rev. B, **69**, 115428, 2004.
12. A. G. BROLO, A. C. SANDERSON, A. P. SMITH, *Ratio of the surface-enhanced anti-Stokes scattering to the surface-enhanced Stokes-Raman scattering for molecules adsorbed on a silver electrode*, Phys. Rev. B, **69**, 045424, 2004.
13. N. HAYAZAWA, T. ICHIMURA, M. HASHIMOTO, Y. INOUE, S. KAWATA, *Amplification of coherent anti-Stokes Raman scattering by a metallic nanostructure for a high resolution vibration microscopy*, J. Appl. Phys., **95**, pp. 2676–2681, 2004.
14. R. C. MAHER, P. G. ETCHEGOIN, E. C. L. RU, L. F. COHEN, *Conclusive Demonstration of Vibrational Pumping under Surface Enhanced Raman Scattering Conditions*, J. Phys. Chem. B, **110**, pp. 11757–11760, 2006.
15. K. KNEIPP, H. KNEIPP, J. KNEIPP, *Surface-Enhanced Raman Scattering in Local Optical Fields of Silver and Gold Nanoaggregates: From Single-Molecule Raman Spectroscopy to Ultrasensitive Probing in Live Cells*, Acc. Chem. Res., **39**, pp. 443–450, 2006.
16. H. KIM, D. K. TAGGART, C. XIANG, R. M. PENNER, E. O. POTMA, *Spatial Control of Coherent Anti-Stokes Emission with Height-Modulated Gold Zig-Zag Nanowires*, Nano Lett., **8**, pp. 2373–2377, 2008.
17. A. JORIO, M. S. DRESSELHAUS, G. DRESSELHAUS, *Carbon Nanotubes in Topics in Applied Physics*, Berlin, Springer, 2008.
18. I. BALTOG, M. BAIBARAC, S. LEFRANT, *Coherent anti-Stokes Raman Scattering on single-walled carbon nanotubes thin films excited through surface plasmons*, Phys. Rev. B, **72**, 245402, 2005.
19. I. BALTOG, M. BAIBARAC, S. LEFRANT, *Single-beam pumped coherent anti-Stokes Raman scattering on carbon nanotubes thin films excited through surface plasmons*, Physica E, **40**, pp. 2380–2385, 2008.
20. S. LEFRANT, I. BALTOG, M. BAIBARAC, *Optical advanced spectroscopic techniques for the study of nano-structured materials: Applications to carbon nanotubes*, Synth. Met., **159**, pp. 2173–2176, 2009.
21. N. DUDOVICH, D. ORON, Y. SILBERBERG, *Single-pulse coherently controlled nonlinear Raman spectroscopy and microscopy*, Nature, **418**, pp. 512–514, 2002.
22. S. H. LIM, A. G. CASTER, S. R. LEONE, *Single-pulse phase-control interferometric coherent anti-Stokes Raman scattering spectroscopy*, Phys. Rev. A, **72**, 041803, 2005.
23. B. VON VACANO, W. WOHLLEBEN, M. MOTZKUS, *Single-beam CARS spectroscopy applied to low-wavenumber vibrational modes*, J. Raman Spectrosc., **37**, pp. 404–410, 2006.
24. X. G. XU, S. O. KONOROV, J. W. HEPBURN, V. MILNER, *Noise autocorrelation spectroscopy with coherent Raman scattering*, Nature Physics, **4**, pp. 125–129, 2008.
25. Y. R. SHEN, *The Principle of Nonlinear Optics*, John Wiley & Sons, Inc., Hoboken, New Jersey, 2002, pp. 242–266.
26. F. EL-DIASTY, *Coherent anti-Stokes Raman scattering: spectroscopy and microscopy*, Vib. Spectrosc., **55**, pp. 1–37, 2011.
27. C. L. EVANS, S. X. XIE, *Coherent Anti-Stokes Raman Scattering Microscopy: Chemically Selective Imaging for Biology and Medicine*, Annu. Rev. Anal. Chem., **1**, pp. 883–909, 2008.
28. A. C. ECKBERTH, *BOXCARS: Crossed-beam phase-matched CARS generation in gases*, Appl. Phys. Lett., **32**, pp. 421–423, 1978.
29. S. LEFRANT, I. BALTOG, M. BAIBARAC, *Surface-enhanced Raman scattering studies on chemically transformed carbon nanotube thin films*, J. Raman Spectrosc., **36**, pp. 676–698, 2005.
30. P. E. WOLF, G. MARET, *Weak Localization and Coherent Backscattering of Photons in Disordered Media*, Phys. Rev. Lett., **55**, pp. 2696–2699, 1985.
31. H. CAO, *Review on latest developments in random lasers with coherent feedback*, J. Phys. A: Math. Theor., **38**, pp. 10497–10535, 2005.
32. E. AKKERMANS, P. E. WOLF, R. MAYNARD, *Coherent Backscattering of Light by Disordered Media: Analysis of the Peak Line Shape*, Phys. Rev. Lett., **56**, pp. 1471–1474, 1986.
33. P. W. ANDERSON, *Absence of Diffusion in Certain Random Lattices*, Phys. Rev., **109**, pp. 1492–1505, 1958.
34. I. BALTOG, M. BAIBARAC, S. LEFRANT, *Abnormal anti-Stokes Raman emission as single beam Coherent Anti-Stokes Raman Scattering like process in LiNbO<sub>3</sub> and CdS powder*, J. Appl. Phys., **110**, 053106, 2011.

Received December 2, 2011